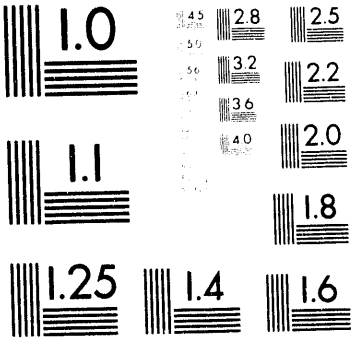
1.0
1.1
1.25
1.4
1.6
1.8
2.0
2.2
2.5
2.8
3.2
3.6
4.0
4.5
5.0
5.6

1 of 1

SAND93-1696
Unlimited Release
Printed August 1993

Distribution
Category UC-906

# Evaluation of the Deployable Seismic Verification System at the Pinedale Seismic Research Facility

D. B. Carr
Seismic Verification Technology Department 9236
Sandia National Laboratories/New Mexico
Albuquerque, New Mexico 87185

MASTER

## Acknowledgment

The author thanks Bobby Corbell for his collaboration on this report. Also a special thanks to Monica Carriaga for retrieving all the data, sometimes not an easy thing to do. Bobby Corbell, Preston Herrington and Jim Walkup gave valuable feedback that improved this report. This work was performed at Sandia National Laboratories supported by the U. S. Department of Energy under contract DE-AC04-76DP00789.

## Contents



## Figures

## Figures (cont)



## Tables

## Executive Summary

The intent of this report is to examine the performance of the Deployable Seismic Verification System (DSVS) developed by the Department of Energy (DOE) through its national laboratories to support monitoring of underground nuclear test treaties. A DSVS was installed at the Pinedale Seismic Research Facility (PSRF) near Boulder, Wyoming during 1991 and 1992. This includes a description of the system and the deployment site (pp 1-3).

We studied system performance by looking at four areas: system noise, seismic response, state of health (SOH) and operational capabilities. System noise (pp 3-7) was studied by comparing velocity spectra to the USGS-Peterson low noise model and the self noise of the instrumentation. A median spectrum on each axis was calculated in each band. We found that the amplitudes of the median spectra are similar to the USGS-Peterson low noise model at frequencies below 0.15 Hz (Fig. 4). Above 0.15 Hz the median spectra are below the low noise model except between 3 and 6 Hz (Figs. 3, 4). The self noise of the system falls below the medians and is not a major component of the background noise. These results indicate that the transfer functions for the seismometers are correct. The overlapping frequency bands have similar responses (Figs. 3,4 and 5).

The affect of wind and seasonal variations on the background noise was also studied (pp 7-10). The effect of increasing wind velocity was only seen on the HF band (Fig. 6) and resulted in the level of the entire spectrum increasing as the noise increased. Peaks around 10, 26, 38 and 48 Hz also increase with increasing wind and we believe they are due to the antenna or fence resonating in the wind. Figures 7, 8 and 9 show the seasonal variation in background noise. The median noise in winter is 2 to 14 dB higher than the median noise in summer at frequencies under 0.9 Hz (Figs. 8, 9), while at frequencies over 1.0 Hz the lowest median noise is in the winter and the highest is in the summer (Figs. 7, 8). We believe the higher noise levels in the summer in the HF band are the result of higher wind velocities in the summer at PSRF.

We studied the seismic response of DSVS using a database of 91 events occurring within 20° of PSRF that had known locations and magnitudes in the NEIS PDE bulletin (pp 10-22). P arrivals were seen for 75 of the 91 events; most events not recorded at PSRF were small magnitude events over 900 km away. $L_g$-waves were seen for almost all the events. Examples of seismic events recorded on DSVS at PSRF are in Figures 11 and 12. Over half of the recorded events were not detected on the HF band until the traces were low passed filtered under 4 Hz (Fig. 13). High pass filtering on the IP band to get rid of the low frequency noise was important to get good arrival times for some events. The local noise obscures the signal for some small magnitude or large distance events since the instrument has such a wide bandwidth.

Magnitudes were calculated using Evernden's WUS magnitude formula and the largest 0-peak amplitude in the first 10 seconds of the P wave for large $m_b$ events. When compared to the NEIS magnitudes the result is a least squares fit to a line with the slope of 1.1 (Fig. 14), indicating the transfer function to convert to displacement is correct. Backazimuth calculations for 70 of the events indicate that to get good estimates the HF band needs to be filtered between 0.5 and 2.0 Hz. The precision of the estimates is 24°

which is not as good as the precision of estimates found for the RSTN stations and Norwegian arrays (Table 3). Figures 16 and 17 show the LP band and the IP band low pass filtered at frequencies under 0.06 Hz to compare the overlapping frequency spans. The traces are similar and no information is lost by using the filtered IP trace, suggesting that the LP band is redundant information.

The attenuation around PSRF was studied by finding the frequency at which the P-wave signal went into the background noise on HFZ and plotting the results against distance and azimuth (Figs. 18, 19). There is an exponential decay of frequency with distance; only $m_b > 6.0$ and $\Delta < 330$ km have energy at frequencies over 30 Hz. Events located east of PSRF are more likely to have energy at frequencies over 20 Hz, which is the result of the different tectonic regimes east and west of PSRF. Since energy over 30 Hz is not seen at PSRF, it may only be necessary to cover the 0.5-30 Hz frequency span with the HF band.

State of health (SOH) information ensures the quality of the data (pp 22-25). The information (Table 4) is valuable and useful in monitoring the system and keeping it running. Only SOH data on the communications needs to be improved. Also, a "semi" expert system that could monitor SOH in real time and warn the operator of problems would increase the usefulness and timeliness of the SOH information.

Funds were not available to evaluate DSVS in an operational mode similar to the evaluation of the National Seismic Stations in RSTN. We would expect however, that the performance of DSVS would be similar to that of RSTN since the same design principles were followed.

## Acronyms and Abbreviations

| | |
|---|---|
| AFTAC | Air Force Tactical Applications Center |
| ARCESS | Arctic Experimental Seismic System |
| DAC | Data Analysis Center |
| DCL | data communications link |
| DHL | downhole logic |
| DOE | Department of Energy |
| DSVS | Deployable Seismic Verification System |
| EUS | eastern United States |
| FIR | finite impulse response |
| FSU | former Soviet Union |
| GPS | Global Positioning Satellite |
| HF | high frequency |
| HPA | high power amplitude |
| HRD | high resolution digitizer |
| IP | intermediate period |
| LP | long period |
| MTBF | mean time between failures |
| MTTR | mean time to repair |
| NEIS | National Earthquake Information Service |
| NORESS | Norwegian Experimental Seismic System |
| NSS | National Seismic Stations |
| NTS | Nevada Test Site |
| PDE | Preliminary Determination of Epicenters |
| PSRF | Pinedale Seismic Research Facility |
| RAMS | Receiving and Monitoring Station |
| RF | radio frequency |
| RSS | Regional Seismic Station |
| RSCP | Regional Station Cumberland Plateau |
| RSNY | Regional Station New York |
| RSON | Regional Station Ontario |
| RSSD | Regional Station South Dakota |
| RSTN | Regional Seismic Test Network |
| RT | receiver/transmitter |
| SOH | state of health |
| TEG | thermoelectric generator |
| UHL | uphole logic |
| USGS | United States Geologic Survey |
| WUS | western United States |

## Introduction

The Deployable Seismic Verification System (DSVS) was developed by the Department of Energy (DOE) through its national laboratories to support monitoring of underground nuclear testing treaties. According to the DSVS Development Plan (1987), the system was developed for the missions of declared test site monitoring associated with a Threshold Test Ban Treaty and general area monitoring associated with a Comprehensive Test Ban Treaty. The most likely deployment would be to the former Soviet Union (FSU). Because of the political climate at the time, DSVS requirements were very similar to those established in the late 1970's for the National Seismic Station (NSS). Those requirements included the following:

1. Provide reliable, high-quality seismographic data for regional and teleseismic analyses.
2. Provide reliable operation so that it would be impractical to induce or hide in failures.
3. Provide evidence of tampering with data and/or equipment.
4. Minimize intrusiveness to the host by minimizing deployment and maintenance activities.
5. Operate in a stand-alone mode with no external power supplied and no commands to the stations.

This report details the evaluation of a Remote Seismic Station (RSS) which was deployed at the Pinedale Seismic Research Facility of the Air Force Tactical Applications Center (AFTAC). Since no funds were available to operate the overall system in a "deployment operations mode" only general conclusions can be made regarding the operational capabilities (e.g. data availability, MTBF, MTTR). However, we were able to choose from the available data to determine the station's seismic data acquisition in which we have high confidence.

## System Description

The elements of the DSVS (Figure 1) are the Remote Seismic System (RSS), the Data Communications Link (DCL), the Receiving and Monitoring Stations (RAMS), and the Data Analysis Center (DAC). RSS is an unmanned seismic station for the acquisition of wide band, three-axis seismic data. There are two versions of RSS. With RSS-1, a three-axis, high-quality seismometer acquires the data and sends it to the downhole logic unit (DHL) where the data is conditioned, digitized and authenticated. State of health (SOH) information is also monitored by the DHL. The RSS-3 configuration has two boreholes, each with an associated seismometer and DHL. For both RSS versions, the uphole logic unit (UHL) merges the data from the DHL with surface state of health data, formats and time tags the data and sends it to the DCL. The primary power source for the RSS is provided by the burning of propane gas and using thermoelectric generators (TEGs) to translate the heat to electrical energy.

The DCL transmits the data from the RSS to RAMS by use of a communications satellite. The remote terminal is a low power RF communications system that transmits the data from the field site to the communications terminal at RAMS. The terminal at

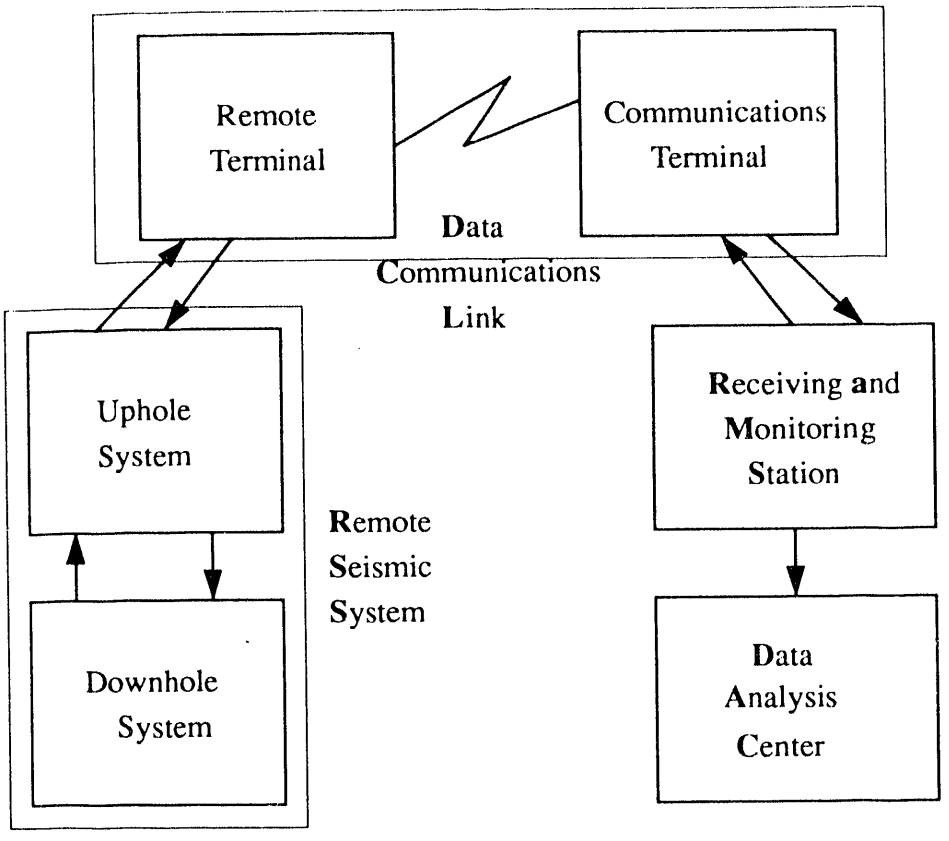


Figure 1. The different components of DSVS include the Remote Seismic Station (RSS) which consists of an uphole system and a downhole system. The data is transmitted from the RSS to the Receiving and Monitoring Station (RAMS) by the Data Communications Link (DCL). Data Analysis Centers (DAC) receive data from RAMS.

RAMS receives the satellite signal and demodulates it so that the data can be used. The function of RAMS is to verify the authenticity of the data received, to assess the operational status of the RSS and to pass the seismic data to analysis centers (DAC). One DAC was developed at Lawrence Livermore National Laboratory, but it is not described or evaluated in this report.

One DSVS station, of the RSS-3 configuration, has been deployed at the Pinedale Seismic Research Facility (PSRF) near Boulder, Wyoming since May 1990. The seismometers are deployed with the holelocks at depths of 42 feet. A Teledyne Geotech S3 seismometer provides 3-axis HF coverage from 0.5 to 50 Hz. The sampling rate is 200 sps with a 24-bit digitizer. A Teledyne Geotech 54000 provides 3-axis coverage in both the IP ((0.01-2.5Hz) and LP(0.02-0.05 Hz) bands. The sampling rate in the IP band is 10 sps with a 24-bit digitizer. In the LP band the data is sampled at 1 sps and a 16-bit digitizer is used.

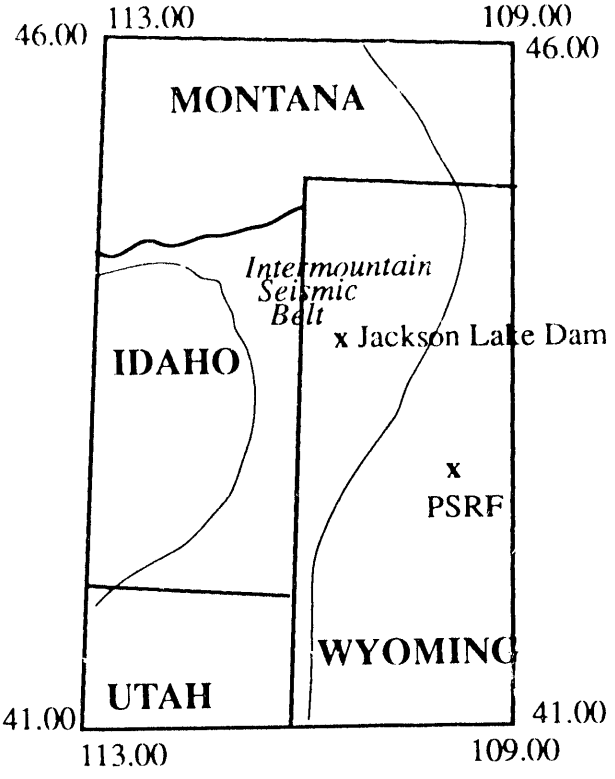


Figure 2. A map showing the location of PSRF in western Wyoming at coordinates 42.77°N and 109.55°W

## Site Description

PSRF is located in western Wyoming on the western front of the Wind River Mountains in the northern end of the Green River Basin (Figure 2) at 42.77°N latitude and 109.55°W longitude. The site for DSVS is situated on the west side of a bluff that strikes approximately 30° west of north. The boreholes were drilled into a saddle with the antenna and equipment shelter ENE of the boreholes. The rocks in the area are granodiorites to porphyritic granite from the 2600 Ma age group. Seismically, the site is approximately 100 km east of the Intermountain Seismic Belt, a band of seismic activity that runs from south central Utah into Montana.

## System Noise

There are various sources of background noise at a seismic station (Taylor, 1981), such as cultural noise (traffic, power supplies, oil industry equipment) and meteorological phenomena (mainly wind). Another source of noise is the self noise of the system itself, i.e. the noise coming from the seismometer, the analog filters and the high resolution digitizers (HRD). This self noise will manifest itself as an additional background noise component.

To evaluate the system noise we collected background noise data on random days from March 1991 through August 1992 at times after 5pm local time. Times were chosen

close to local midnight to reduce the cultural noise effects. Two hundred and fifty seconds of HF data, 500 seconds of IP data and 5000 seconds of LP data were collected on all three axes for analysis of each band. Spectra were calculated on all the data using 512 point Hanning windows with 0.5 overlap over the entire data window. A median spectrum was calculated for the axes in each band and compared to a conservative estimate of the self noise of the system. The medians were also compared to the USGS-Peterson low noise model, a composite from different world-wide stations of the lowest measurements of noise in a particular frequency band. All spectral analysis was done in velocity.

One hundred and forty four spectra in the HF band were used to calculate the HF medians shown in Figure 3. The general shape of the spectra follow the USGS-Peterson low noise model. with steep fall-off of 75 dB per decade between 0.5 and 1.0 Hz. From 1.0 to 4.0 Hz the spectra flatten and then fall-off again (30 dB per decade) from 4.0 to 50.0 Hz. The steep roll off between 50 and 70 Hz is due to the FIR filter in the HRD. The median spectra are below the USGS-Peterson low noise model at all frequencies except a band between 3 and 6 Hz. The horizontal axes have higher noise in this band than the vertical axis. Because the background noise level and USGS-Peterson low noise model fit well together we can be confident that the transfer function for the seismometer is correct. We also found that PSRF is a quiet site at frequencies over 6 Hz. The modeled self noise of the system is below the median spectra until approximately 15 Hz and crosses the USGS-Peterson low noise model at around 32 Hz. We used a conservative estimate of the analog filter noise in the self noise model, and feel that the data are good at frequencies up to 40

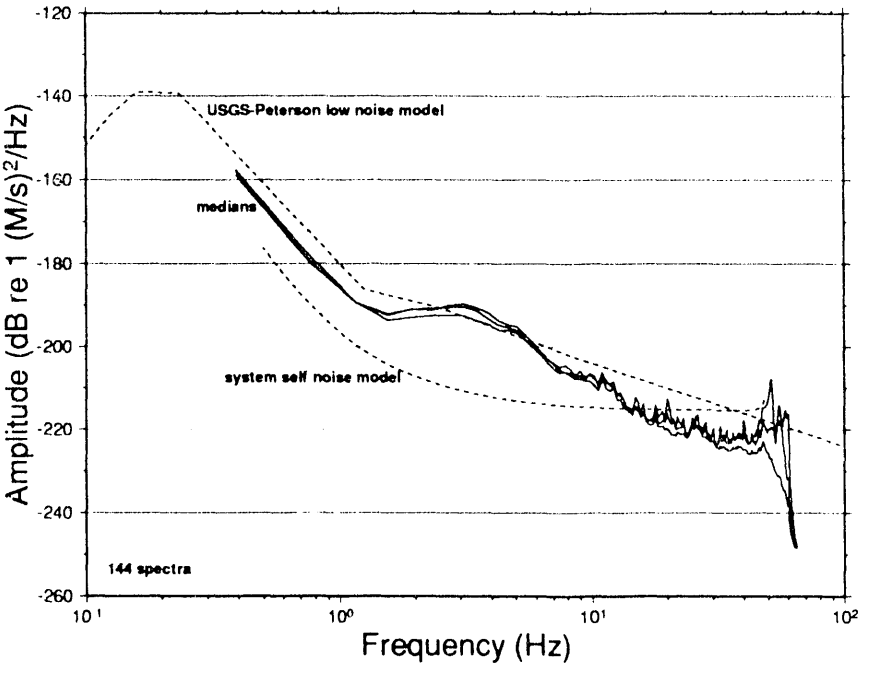


Figure 3. Median velocity noise spectra for the vertical, north and east components of the HF band, calculated from 144 spectra.

Hz. If the background noise is independent there should be no coherency between the three axes. We only found coherency in the HF band at four specific frequencies: 25, 38, 48 and 55 Hz.

One hundred and forty three spectra in the IP band were used to calculate the medians shown in Figure 4. The general shape of the spectra roughly follow the USGS-Peterson low noise model. The spectra increase at 55 dB per decade from 0.02 to 0.15 Hz. They peak at 0.15 Hz, then roll off at 70 dB per decade to 1.0 Hz. The spectra flatten from 1.0 Hz to 2.5 Hz, where the data roll off due to the HRD FIR filter. The horizontal axes do not have as good performance as the vertical axis at frequencies less than 0.04 Hz, because of a higher noise floor at 0.01 Hz on the horizontal modules. The median IP spectra are below the USGS-Peterson low noise model at frequencies over 0.15 Hz. At frequencies less than that, the median and USGS-Peterson low noise model have similar amplitudes, indicating the transfer function for the seismometer is good. The modeled system self noise is below all the spectra over the entire frequency band except for the vertical axis at the low end of the band (0.01-0.02 Hz). Since we used a conservative self noise model, the data at these frequencies should be good. The two small peaks at 1.0 and 2.0 Hz on the E-axis are due to the coupling through the borehole cables of the system electronics.

One hundred and twenty four spectra in the LP band were used to calculate the medians shown in Figure 5. The general shape of the spectra from 0.02 to 0.05 Hz roughly follow the USGS-Peterson low noise model. On the vertical axis the spectrum is flat from

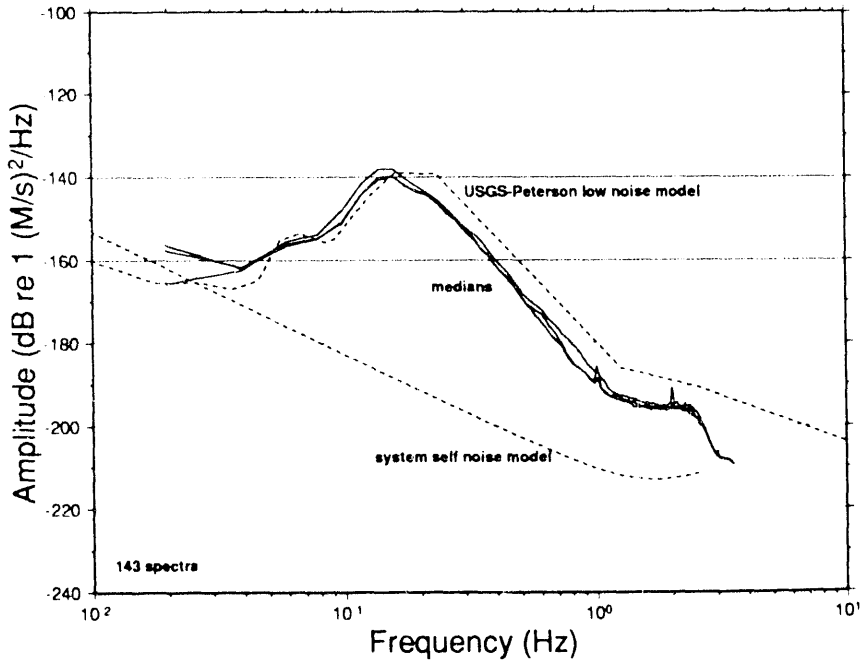


Figure 4. Median velocity noise spectra for the vertical, north and east components of the IP band, calculated from 143 spectra. The small peaks at 1.0 and 2.0 Hz on the E-component are due to modulation of the system electronics.

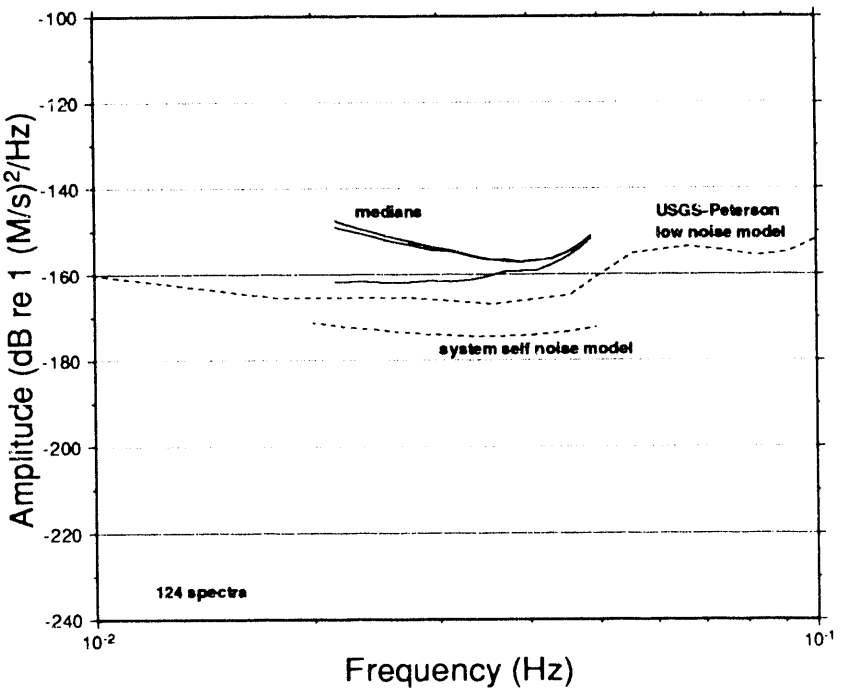


Figure 5. Median velocity noise spectra for the vertical, north and east components of the LP band, calculated from 124 spectra.

0.02 to 0.04 Hz, but on the horizontal axes the spectra decrease at a rate of 45 dB per decade. This is because the horizontal modules have a higher noise floor at frequencies around 0.01 Hz than the vertical module. On all three axes the spectra increase at approximately 120 dB per decade between 0.04 and 0.05 Hz. The median spectra are above the USGS-Peterson low noise model at all frequencies in the LP band. The modeled self noise of the system is below all the spectra and has a similar shape. Part of the discrepancy in this band is due to the performance of the 16 bit digitizer, which actually performs as a 14 bit digitizer.

DSVS was designed with overlapping frequency bands. The HF and IP bands overlap in the frequency range of 0.5 to 2.5 Hz. In this frequency span the medians in the HF band and IP band are very close in amplitude (Figures 3 and 4). The IP band is slightly lower (3 to 7 dB) than the HF band, but the shape of the medians is the same. In both bands the medians are below the low noise model. The two seismometers recording data from 0.5 to 2.5 Hz are both doing an adequate job. The IP and LP bands overlap in the frequency range of 0.02 to 0.05 Hz (Figures 4 and 5). In this frequency span the medians in the LP band are 3 to 8 dB above the median in the IP band and all are above the low noise model. The shape of the medians are similar, except there is more of an increase in slope from 0.035 to 0.05 Hz in the LP band.

The IP and LP bands are recorded with the same seismometer, a 54000. The differences seen in the spectra are due to analog filters and digitizers used to collect the data.

The comparison of the two bands points out that the IP band covers the entire LP band and does a slightly better job of recording the data. This suggests that a single band, using modern low noise 24 bit high resolution digitizers would be adequate for covering the frequency span of 0.01 to 2.5 Hz.

## Meteorological Phenomena

Wind velocity is a major meteorological phenomenon that can cause an increase in background noise levels. Winter storms and spring run-off have also been cited as reasons for increased noise levels (Basham and Whitman, 1966; Smart and Sproules, 1980; Fyen, 1987). The changes to the background noise due to meteorological phenomena can be site specific, but are important to study to determine their effect on system performance. We also are interested in determining the advantage of having anemometers installed with DSVS at PSRF.

To look at the effect of wind, the noise data were separated into four groups based on the average wind speed from the anemometer at the time the data was collected. Median spectra were calculated for wind speeds less than 0.1 mph, between 2.0 and 5.0 mph., between 8.0 and 15.0 mph and greater that 15.0 mph. Seasonal variation was studied by separating the data into different seasons (Table 1), and comparing the median spectra calculated in each frequency band.

Using the anemometer located north of the antenna, we found that as wind speed varied from 0 to 30 mph, only the HF band had any noticeable changes in the background noise. In Figure 6, median spectra in the HF band have been calculated using spectra from times with different wind speeds. As the wind speed increases, the level of the entire spectrum increases and peaks around 10, 26, 38 and 48 Hz are larger. We believe that these peaks are due to the wind blowing on the antenna located 15 meters ENE of the borehole or through the fence surrounding the area, causing them to resonate. Backazimuths calculated from these peaks indicate that the source of all peaks is from 30° to 60° east of north, which corresponds well to the antenna. The broad peak from 9 to 12 Hz, is also seen when the wind is very low, so we suspect oil jacks in the area may be the source of this noise peak. There can be differences of over 10 dB between noise levels with wind speeds less than 1.0 m.p.h. and noise levels at the windiest periods. It is only because we have anemometers installed at the station that we can correlate wind at PSRF with the background noise.

Figures 7, 8 and 9 show the seasonal variation seen in the noise levels at DSVS at PSRF. The median noise in the winter is 2 to 14 dB higher than the median noise in summer at frequencies less than 0.9 Hz (IP, LP bands). The spring and autumn median noise levels are very close, and fall in-between winter and summer. At frequencies over 1 Hz

Table 1-Breakdown of seasons used for seasonal variation

| | |
|---|---|
| Spring: | March, April and May |
| Summer: | June, July and August |
| Autumn: | September, October, November |
| Winter: | December, January, February |

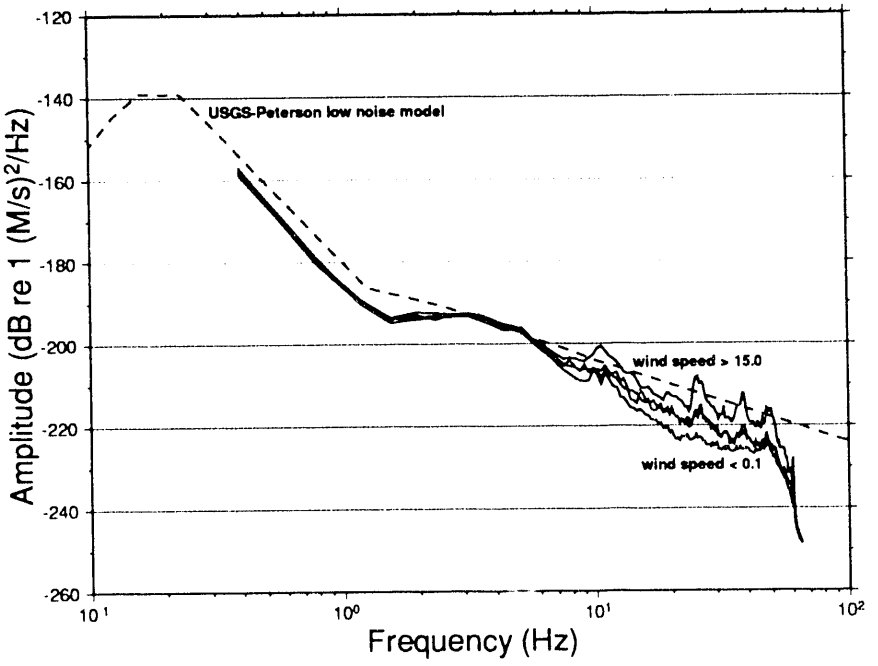


Figure 6. Median velocity noise spectra for different values of average wind speed on the HF band.

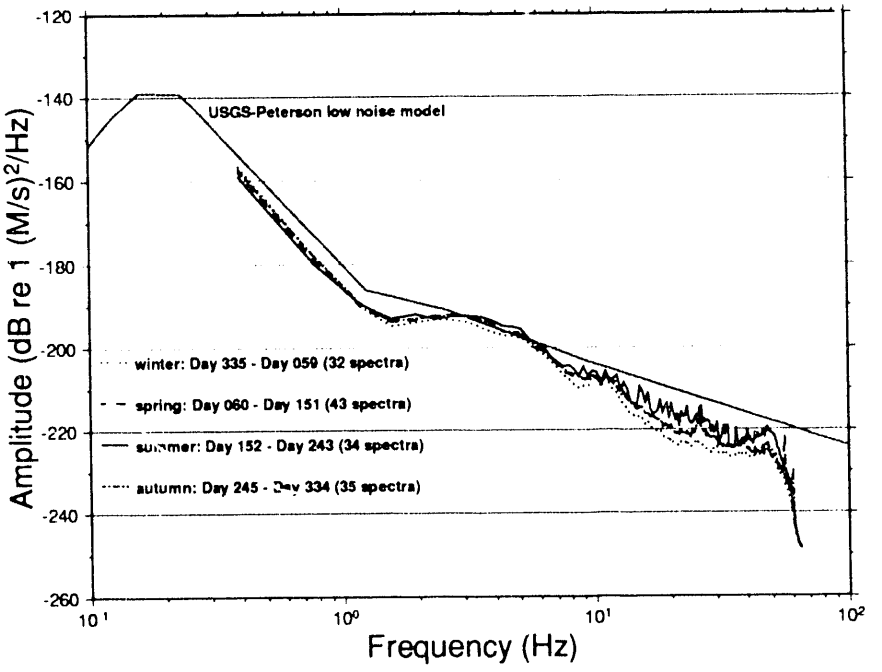


Figure 7. Median velocity noise spectra for different seasons on the HF band. Over frequencies of approximately 2 Hz, the summer noise level is the highest and the winter noise level is the lowest.

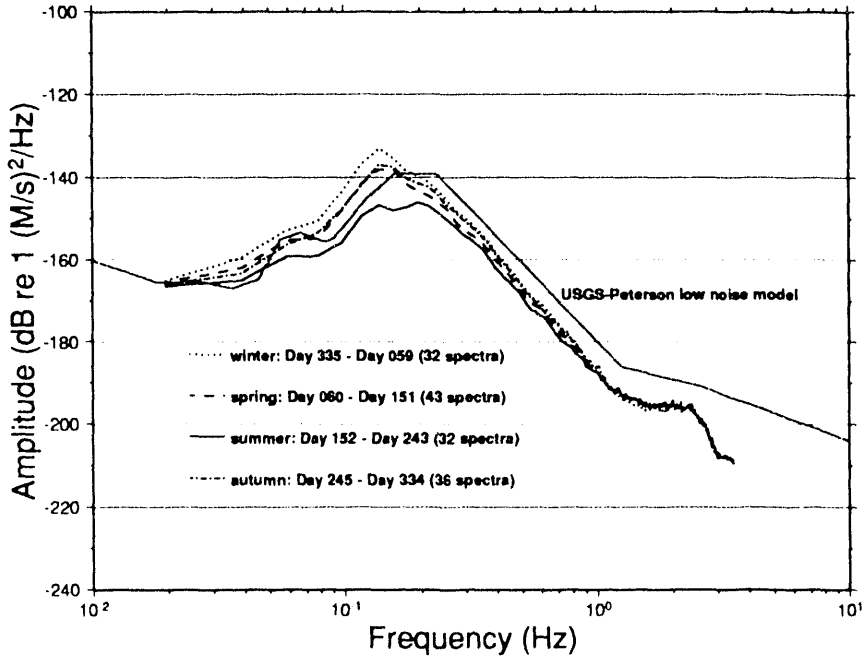


Figure 8. Median velocity noise spectra for different seasons on the IP band. The winter noise level is the highest and summer noise level is the lowest over most of the frequency range in this band.

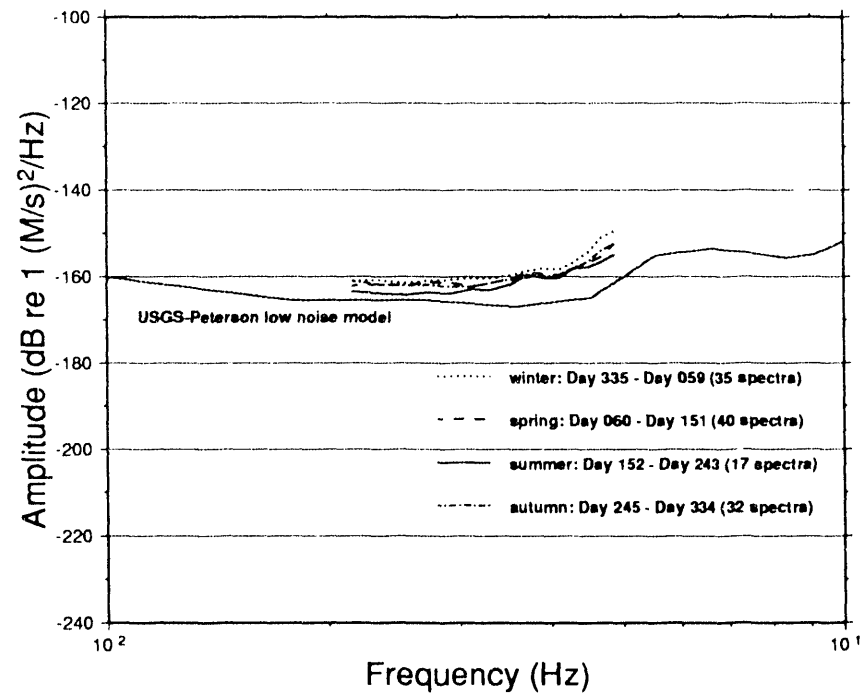


Figure 9. Median velocity noise spectra for different seasons on the LP band. The winter noise level is the highest, summer noise level the lowest over this frequency band.

(HF band), the lowest median noise is in the winter; the highest median noise is in the summer; and the median noise in spring and autumn are almost identical and fit in-between. Meteorological disturbances during the winter have been considered to be the major factor as to why winter noise levels are high at the longer periods (Basham and Whitman, 1966; Smart and Sproules, 1980). In Norway, Bungum et al. (1971) and Ringdal and Bungum (1977) found that noise levels were highest in the fall and lowest in summer for frequencies under 2 Hz. Fyen (1987) extended the frequency band to 20 Hz and studied the noise at specific frequencies for a period of a little longer than a year. He found the highest noise levels at frequencies over 2 Hz were in the spring and contributed this increase to the snow melting and increasing the water flow in nearby rivers. At PSRF, we looked at the average wind speed in the different seasons to see if an increase in wind during the summer could explain the higher noise level at the higher frequencies. In our data set, the average wind speed in the winter is very low; it is less than 1.0 mph for 88% of the events. It is only in the summer when the average wind speed is over 15 mph. In Figure 6 we see a difference of 5 to10 dB between the median spectra for wind speeds over 15 mph and wind speeds less than 1.0 mph. The higher noise levels in the summer can be accounted for by the increase in velocity of the wind.

## Seismic Response

It is important to determine how well DSVS at PSRF records seismic events. Some of the response of the instrument is site specific, but we need to determine if there are any limitations in the instrumentation. To evaluate the seismic response we studied the response of the system to known event data. This includes looking for specific arrivals, determining amplitude response and finding the backazimuth estimation capabilities of the system. We also wanted to determine the type and amount of data processing needed to look at the events, compare the overlapping frequency bands and evaluate the importance of both recording the data to 60 Hz and the LP band.

A database of 91 events occurring within 20° of PSRF was collected to evaluate the response of the system. The events have known locations from the Preliminary Determination of Epicenters (PDE) bulletin of the National Earth-quake Information Service (NEIS). A map of the events is in Figure 10. The magnitudes o. the events include local magnitudes (ml) from various networks in the western U.S. that range from 2.0 to 4.9, and body-wave magnitudes ($m_b$) calculated by NEIS. The $m_b$ magnitudes range from 2.5 to 6.4. Since we had known locations for the events we started by looking for the different phases ($P_n$, $P_g$, $S_n$ and $L_g$) to see if they arrived at the times they were supposed to according to the Jeffrey-Bullen tables. The highest zero-to-peak amplitude in the first 10 seconds was found and used to calculate a magnitude with Evernden's western United States (WUS) magnitude formula (Evernden, 1967). Any processing of the data, i.e. filtering, was documented and the frequency at which the signal went into the background noise on the vertical axis of the HF band was found to get an idea of the attenuation around PSRF. The response of the overlapping frequency bands was compared both spectrally and by comparing the traces. And finally, a backazimuth was calculated following the method of Walck and Chael (1991).

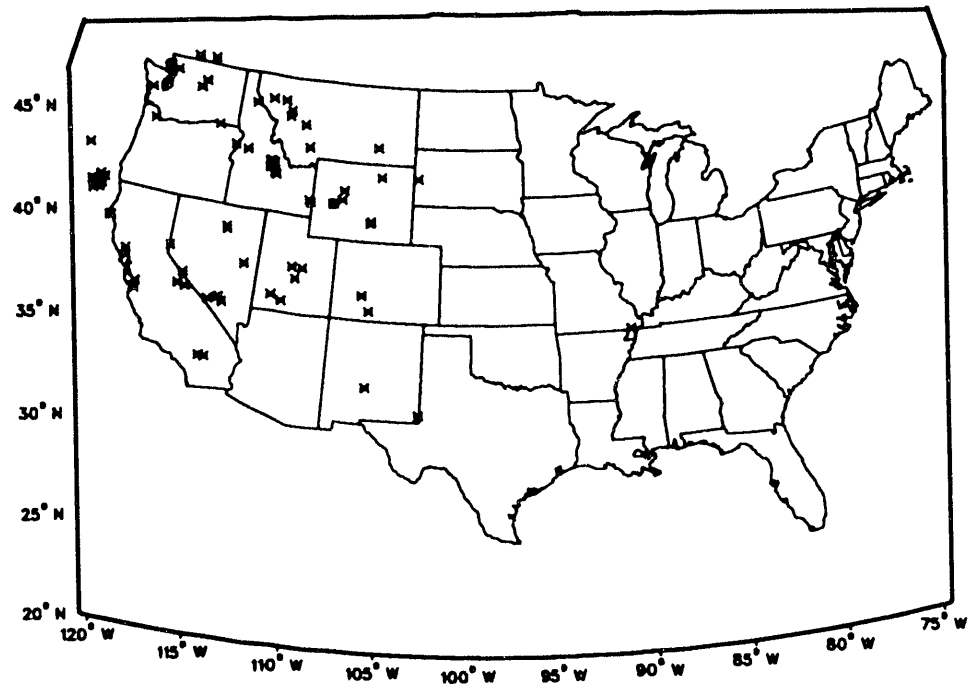


Figure 10. Map of events used to study the seismic response of DSVS. All the events (x) are within 20° of PSRF (box).

P-arrivals were seen for 75 of the 91 events in the database. Most of the sixteen events that were not recorded on DSVS at PSRF were over 900 km away and had small local magnitudes (3.0-3.5). Figures 11 and 12 have examples of events recorded at DSVS. The first event (Fig. 11) is a local magnitude 3.0 earthquake occurring 236 km east of PSRF. Good $P_n$ and $L_g$ arrivals are seen on both the HF and IP bands, but there is nothing on the LP band. Figure 12 shows an earthquake off the northern coast of California that has an $m_b = 6.0$. The $L_g$ arrival is seen clearly on the LP band for this event, which is 1262 km away. No $P_g$ arrivals were seen for events at distances over 1150 km, which follows the typical $P_g$-distance relationship. For 51 events in the database there was no $S_n$ arrival. Other authors have noted the absence of observations of $S_n$ in the WUS, (Molnar and Oliver, 1969; Der et. al., 1982) and attribute it to upper mantle attenuation or discontinuity of the waveguide. At PSRF, the $S_n$-wave was mostly seen for events at short distances (<250 km) and for high $m_b$ events more than 1200 km away. The $L_g$-wave was seen for almost all the events in the database. Events with no $L_g$-wave were those at distances less than 120 km from PSRF and some events off the Oregon and northern California coasts.

## Data Processing

We documented the data processing needed to detect events with DSVS at PSRF to determine how easily events were detected and what aspects of the system hinder detec

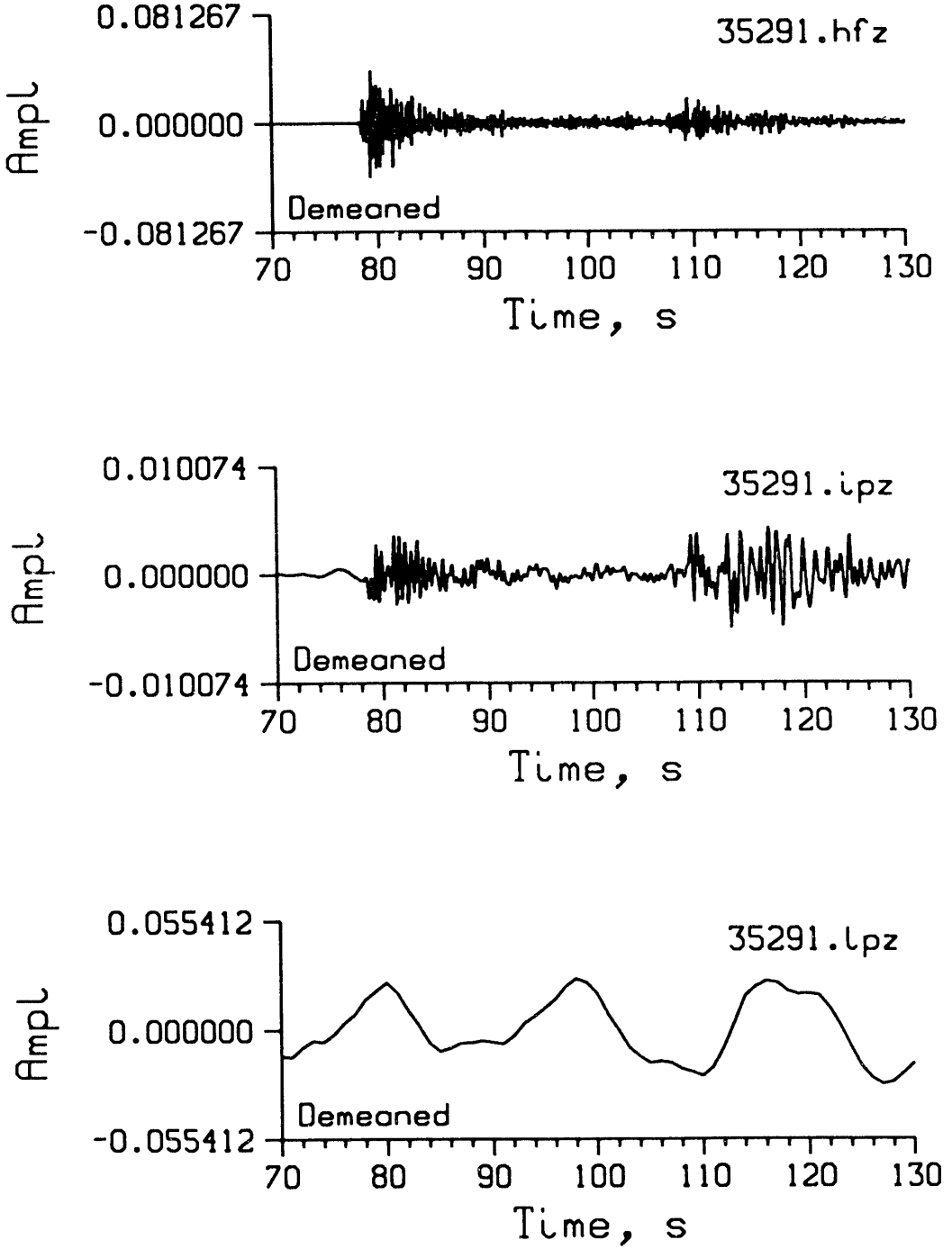


Figure 11. A local magnitude 3.0 earthquake occurring 236 km east of PSRF on December 18, 1991. Good $P_n$ and $L_g$ arrivals are seen on the HF and IP bands, but there is nothing on the LP band.

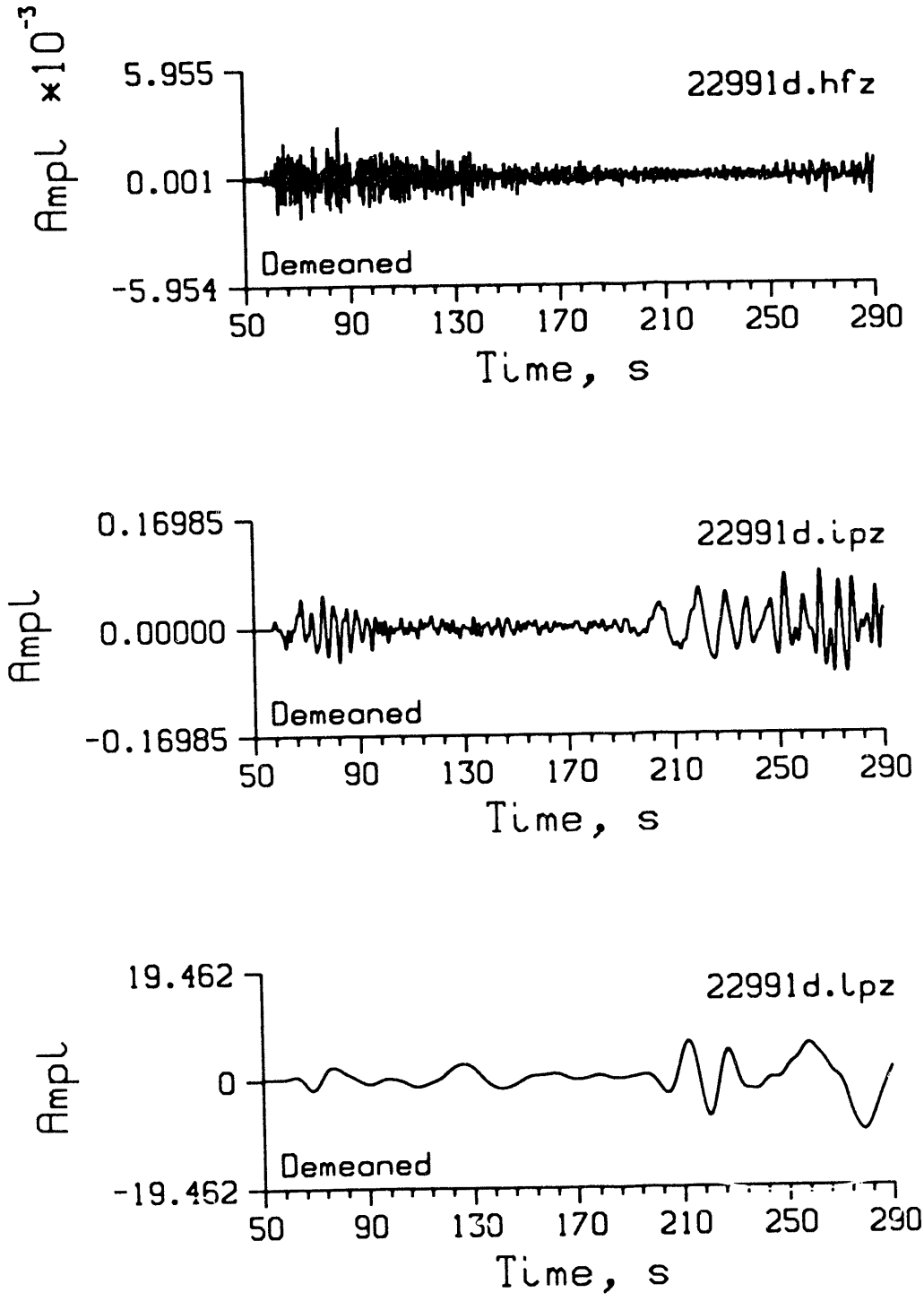


Figure 12. A $m_b$ = 6.0 earthquake occurring off the coast of California, 1262 km from PSRF on August 17, 1991. Good $P_n$ arrivals are seen on all bands, and good $L_g$ is seen on IP and LP.

tions. Thirty-six events were seen without filtering on the HF band. These included all the events occurring within 350 km of PSRF, all events with $m_b$ over 4.6 and all events located east of PSRF (azimuths < 163°). The remaining 39 events were only seen on the HF band when the data was low pass filtered at frequencies less than 4 Hz. Figure 13 shows a $m_b$ = 4.3 earthquake located over 1200 km west of DSVS that was not detected on the HF band until the data was filtered. There is no indication of a seismic event on the demeaned trace of the data. Filtering is also needed on the IP band to get rid of the low frequency noise. For a large number of the 39 events, high pass filtering on the IP band was needed to get good arrival times. The LP band in Figure 13 shows a good $L_g$ arrival. For this particular event, the LP band has the best detection. What we found was that preprocessing of the data was needed for slightly over one half of the events detected on DSVS. A lot of the preprocessing was necessary because we are using wide bandwidths to record the data. For small magnitude events and events at large distances, the local high frequency noise obscures the signal.

## Amplitude-Magnitude Relationship

The relationship of the zero-peak amplitude of an event and the magnitude depends upon the distance from the event to the recording station and the tectonic regime. In general, at PSRF the largest zero-peak amplitudes measured in volts during the first 10 second of the P-arrival are seen for events less than 300 km away and for events more than 800 km away with NEIS $m_b$ magnitudes over 5.0. For the large NEIS $m_b$ events occurring over 800 km west of PSRF, magnitudes were calculated using Evernden's WUS magnitude formula:

$$m_b(\text{WUS}) = -7.55 + 1.2[\log(A/T) + 3.04(\log(\Delta)]$$

where A is the zero-peak amplitude in nanometers, T is the period in seconds and $\Delta$ is the distance in kilometers. When compared to the NEIS $m_b$ magnitudes, the result is a least-squares fit to a line with a slope of 1.1 (Figure 14). The magnitudes measured by DSVS using the WUS formula are a good match to the NEIS magnitudes, so the transfer function used to convert the data to displacement is correct.

## Backazimuth Estimation

To determine the accuracy of backazimuths of events calculated from DSVS at PSRF, we followed the method of Walck and Chael (1991). The seismograms were filtered with a 4-pole Butterworth causal filter and backazimuths calculated over a specific time span. Errors were found by subtracting the azimuth determined from the PDE locations from the calculated azimuths. The PDE locations are regarded to be accurate to 10 to 16 km, so the reference backazimuths should be a reliable standard with which to compare the three-component backazi-muth estimate. Different time spans, filter and methods were used to calculate backazimuths (Table 2). Methods used were Magotra et al. (1987) and Roberts et al. (1989). They use different constraints on the nature of the polarization of P-arrivals and background noise. Estimates are close for strongly polarized signals. Backazimuth calculations were made for 70 of the 91 events in the data base. The best results

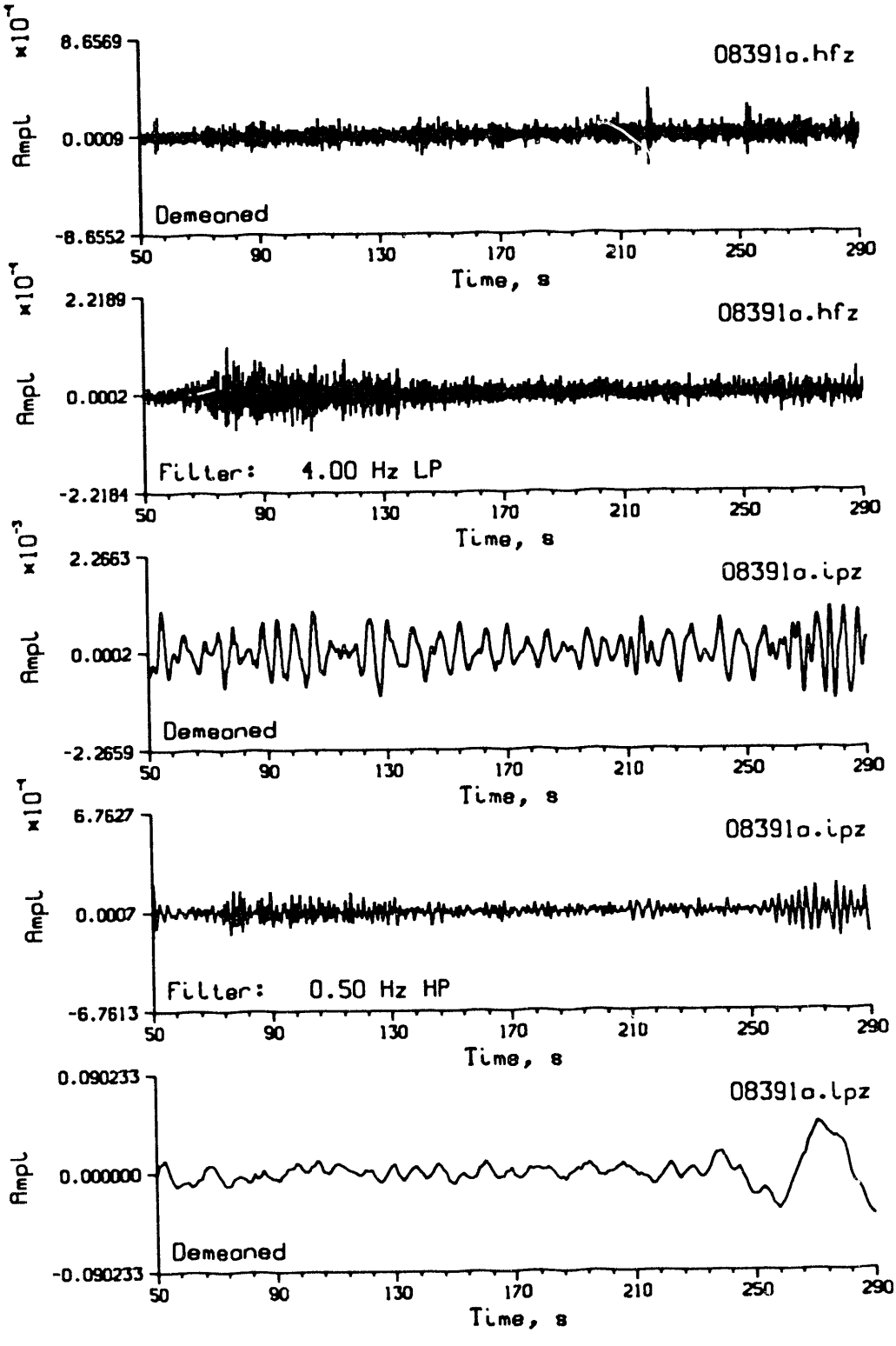


Figure 13. Traces of a $m_b$ = 4.3 earthquake occurring 1200 km west of PSRF show how filtering of the HF band can be important when detecting events. This event was first detected by finding the $L_g$ arrival on the LP band.

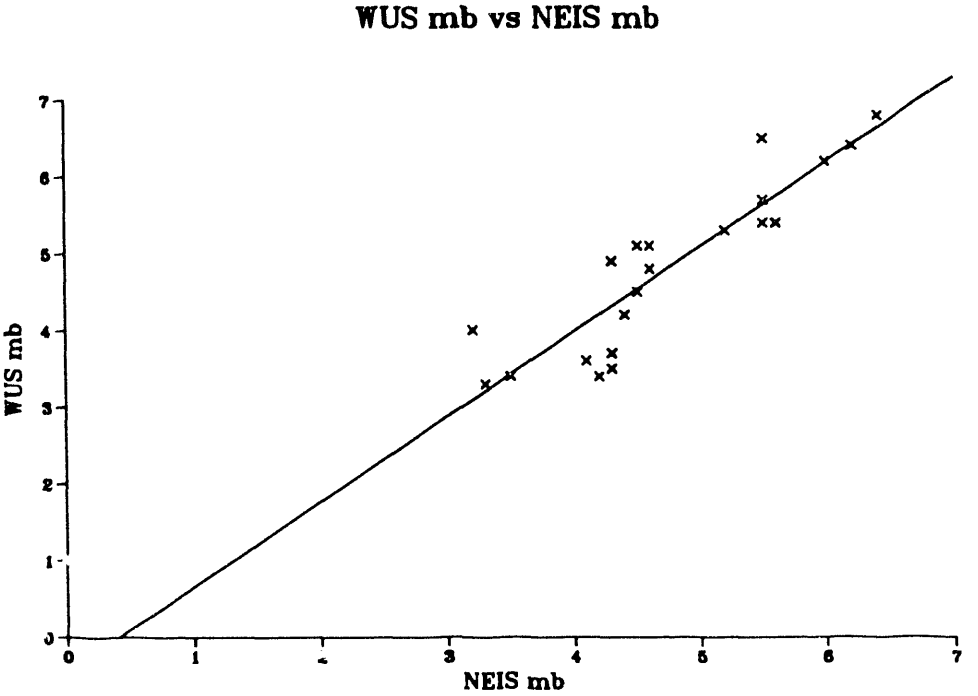


Figure 14. NEIS $m_b$ magnitudes compared to magnitudes calculated using Evernden's WUS magnitude calculation. The least-squares fit has a slope of 1.1.

occur when the data is filtered at low frequencies (0.5-2.0 Hz) and calculated over an eight second time window. Results using both methods are in Figure 15. The Magotra et al. (1987) method gives azimuth errors that range in absolute value from 1.6° to 175.1°. The mean or bias is 5.0° and the precision is 38.0°.The precision and bias decrease slightly using the method by Roberts et al. (1989); 4.2° and 37.1° respectively. The absolute values of the errors range from 0.2° to 162.2°. If another station is used along with DSVS at PSRF to determine locations then the ambiguity in direction if the error is greater than 90° can be resolved. If errors are rotated to be within ±90°, the mean error increases but the precision is better. The precision improves to 24° using Magotra et al (1987), and is 27.3° using the method by Roberts et al. (1989). We compared the backazimuth estimation capabilities of DSVS to the RSTN stations in Walck and Chael (1991) and results from the NORESS (Bame et al, 1990) and ARCESS (Carr, in prep.) arrays in Norway (Table 3). Most of the RSTN stations and both of the arrays have better precision than DSVS at PSRF. The site with the poorest precision is RSSD which Walck and Chael attribute to dis

Table 2. Filters, time spans and methods used to calculate backazimuths

| Filters | Time spans | Methods |
|---|---|---|
| 0.5-2.0 Hz | 2 seconds | Magotra et al. (1987) |
| 0.5-4.0 Hz | 5 seconds | Roberts et al. (1989) |
| 0.5-8.0 Hz | 8 seconds | |
| 2.0-4.0 Hz | | |

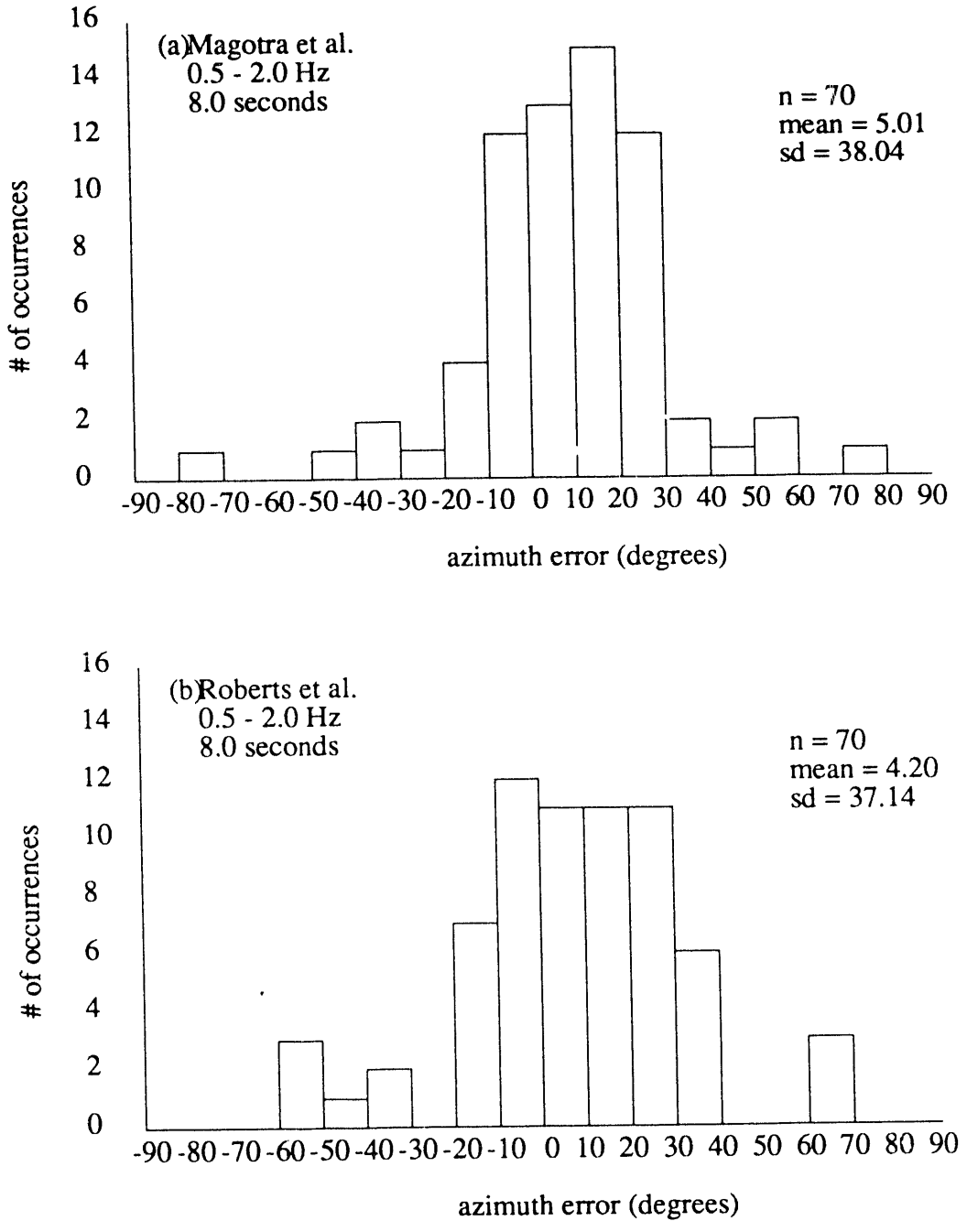


Figure 15. (a) The range of errors in backazimuth for 70 events around PSRF using the method of Magotra et al. (1987), 0.5-2.0 Hz filter and 8 second time window. The mean is 5.01° and the standard deviation is 38.04°. (b) The range of errors in backazimuth for 70 events around PSRF using the method of Roberts et al. (1989), 0.5-2.0 Hz filter and 8 second time window. The mean is 4.20° and the standard deviation is 37.14°.

torting of the incoming seismic energy at the site. Looking closer at DSVS at PSRF, we found that backazimuth errors are larger for events with signal-to-noise ratios less than 10, and we also saw an azimuthal dependence in error. Events located NE of PSRF (azimuths

Table 3. Precision of backazimuth estimation

| Station | Precision | Station | Precision |
|---|---|---|---|
| DSVS | 24.0° | RSCP | 13.5° |
| RSNY | 10.6° | NORESS | 11.1° |
| RSON | 21.3° | ARCESS | 16.9° |
| RSSD | 27.6° | | |

less than 112°) have an average mean error of 12.5°. The average mean error was 29.8° for events located at azimuths over 290°. Because of the differences in backazimuth error with SNR and azimuth, we believe the poor precision achieved when calculating backazimuths with DSVS at PSRF is due to site characteristics, not the instrumentation.

## Overlapping Frequencies

The overlapping frequency span in the IP band and LP band were compared by low pass filtering the IP band at frequencies under 0.06 Hz. Filtered IP traces and LP traces are shown in Figures 16 and 17. The event in Figure 16 is a nuclear explosion from NTS. The characteristic long period signal is seen on both the LP band and the filtered IP band. An earthquake occurring 625 km SSW of PSRF is shown in Figure 17. The $L_g$ phase arrives at around 160 sec where the high frequency energy component starts. The two bands are not identical for either event, because of the affects of filtering, the differences in the sample rate and for the NTS event, gain ranging on the LP band. However, the traces are very similar, and no information is really lost by filtering the IP band. The response of the two bands would be the same if inverse filtering was applied to the IP band and then the data filtered by the LP band response. It was more difficult to compare the overlapping frequency span in the HF and IP bands. When both bands are bandpassed between 0.5 and 2.5 Hz, the HF band has less low frequency energy because of the sharp roll off at 0.5 Hz used to shape the HF band. The response of the two bands would be the same however, if inverse filtering was applied to the IP band and the data filtered by the HF band response.

## Importance of Broadband Recording

The frequency response of DSVS at PSRF was studied by determining the frequency at which the P-wave signal went into the background noise on HFZ for each event. The majority of events did not have energy at frequencies over 20 Hz. When the frequency at which the signal goes into the background noise is plotted against distance (Figure 18) we see an exponential decay of frequency with distance. Except for large magnitude events ($m_b > 6.0$), we don't see energy over 30 Hz unless the distance is less than 330 km. There also appears to be a difference in frequency response with azimuth (Figure 19). Events to the east of PSRF are more likely to have energy at frequencies over 20 Hz than events west of PSRF. The reason for this is the difference in the tectonic regimes that are east and west of PSRF. The eastern United States (EUS) is a stable shield region compared to the tectonically active WUS. The complex geology west of PSRF attenuates the higher frequencies at a faster rate. Another area where frequency attenuation has been studied

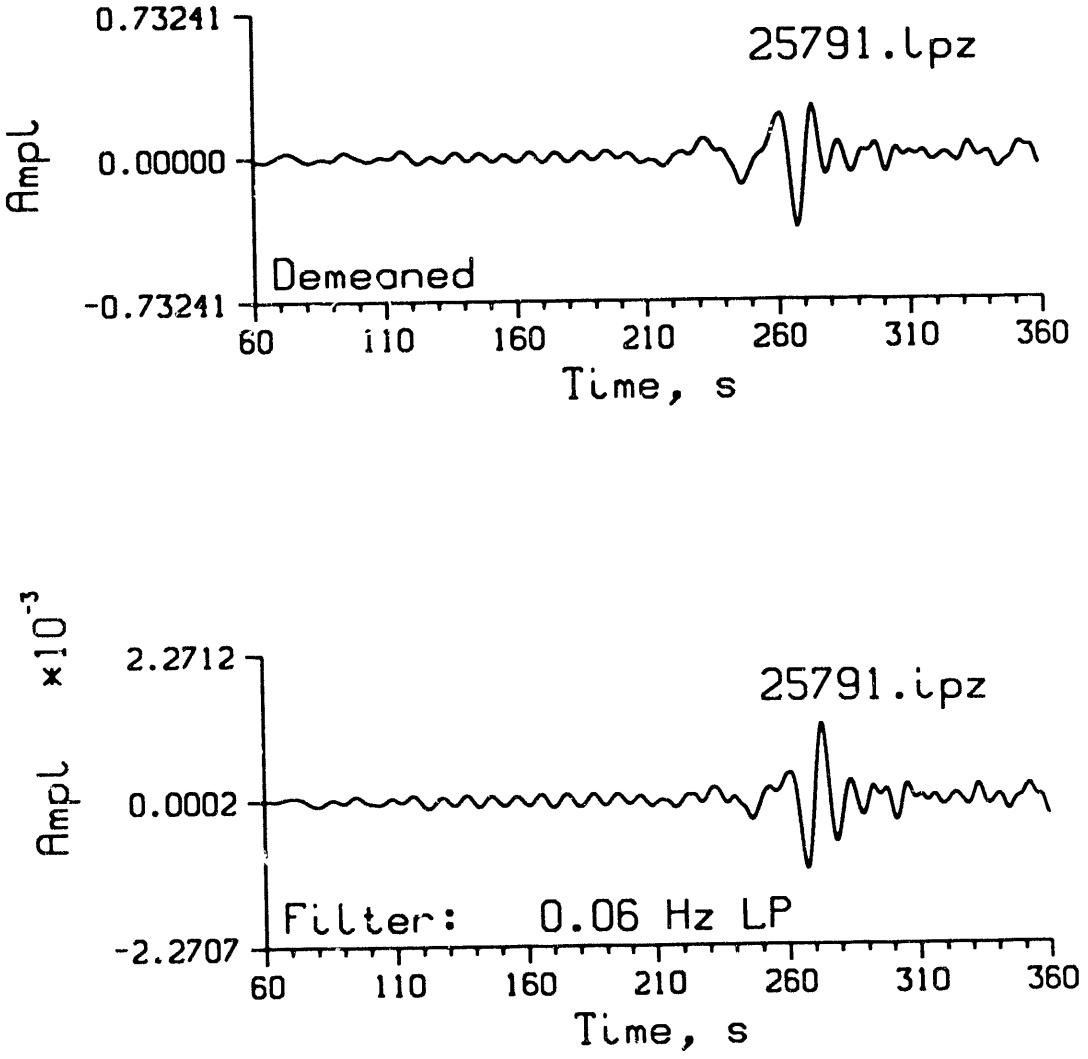


Figure 16. A NTS nuclear explosion recorded on DSVS at PSRF on the LP band and low pass filtered (0.06 Hz) IP band.

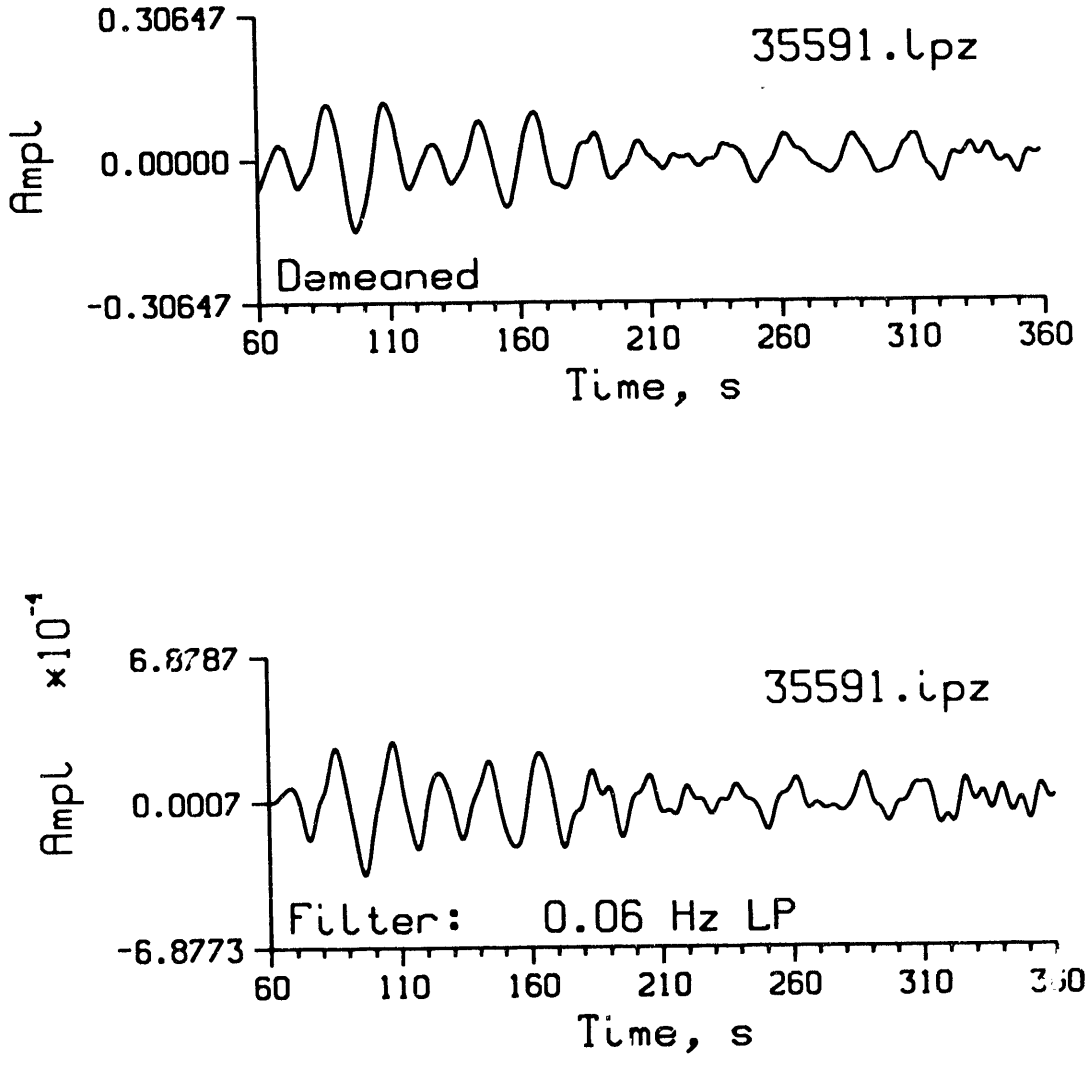


Figure 17. An earthquake occurring 625 km SSW of PSRF recorded on the LP band and low pass filtered (0.06 Hz) IP band.

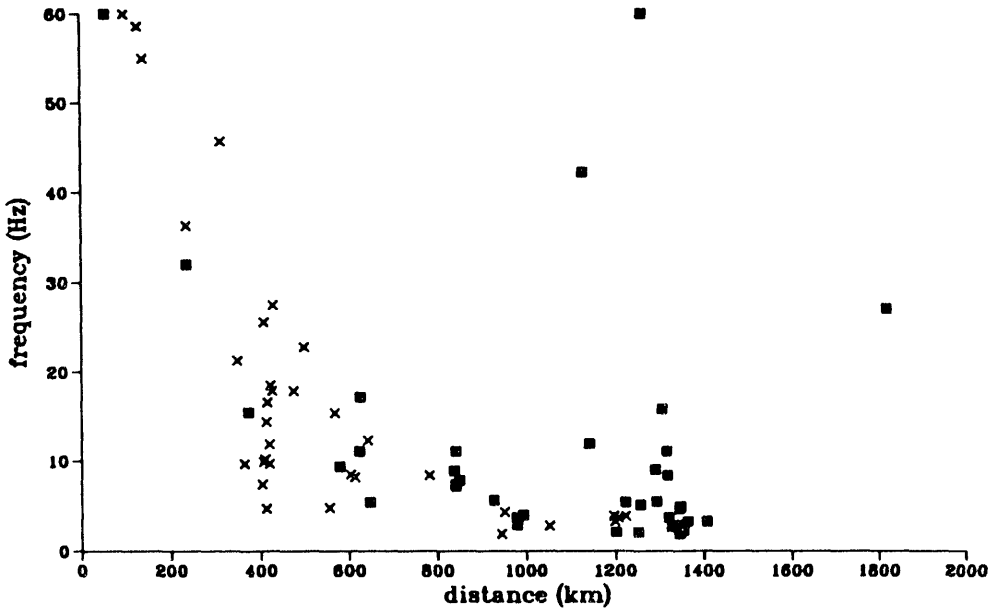


Figure 18. The frequency where the signal goes into the background noise on HFZ compared to the distance from the event location to PSRF (ml(x) and $m_b$(box)). There is an exponential decay in frequency with distance except for a few large magnitude events. The event at 1262 km with a frequency of 60 Hz is a 6.0 $m_b$ earthquake off the northern California coast. The event at 1130 km with a frequency of 42 Hz is a 6.2$m_b$ earthquake near Yucca Valley California. The event at 1820 km with a frequency of 27 Hz is a 4.4 $m_b$ earthquake from the New Madrid fault zone.

was in southern Norway (Bame, 1989). The magnitude range of the events used in the Norwegian study are local magnitudes between 0.2 and 3.5. The signals have energies out to 30 Hz for events out to distances of 1400 km. Energies over 30 Hz are not seen unless the event occurs less than 600 km from the seismometer. In Norway, another stable continental shield, we see that smaller magnitude events have higher energy content than events in the mid-continent and WUS at similar distances.

Even in a good area for high frequency propagation such as Norway, frequencies over 30 Hz are not valuable unless the event is close to the seismometer. The local high frequency noise can obscure the signal of events with small magnitudes and at large distances. Frequencies out to 50 Hz were implemented in DSVS because it was thought that earthquakes and nuclear explosions could be discriminated using frequencies out to 100 Hz. In a study by Bame-Carr (1992) looking at known earthquakes and chemical explosions in Norway recorded to 50 Hz, there was no difference between the two. At NTS, Chael (1988) found that spectral differences between earthquakes and nuclear explosions could be seen at frequencies from 10 to 30 Hz. At DSVS, events in the WUS don't have energy over 20 Hz unless it is a large magnitude event. The nuclear explosions from NTS in the database only have energy out to between 7 and 10 Hz at PSRF, so any attempts at discrimination at frequencies at 15 to 30 Hz cannot be done.

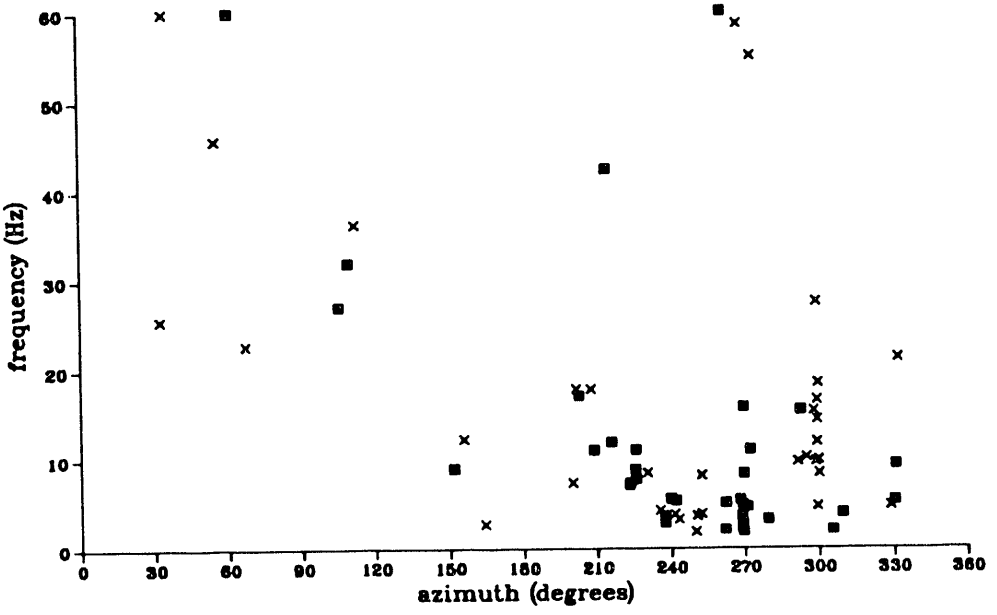


Figure 19. The frequency where the signal goes into the background noise on HFZ compared to the azimuth of the event location to PSRF (ml(x) and $m_b$(box)). Except for $m_b$ = 6.2 and $m_b$ = 6.0 earthquakes and two events within 150 km west of PSRF, events to the east of PSRF have higher frequency energy than events to the west of PSRF.

Looking at the overlapping frequency spans and high frequency attenuation suggests that only two frequency bands are necessary for DSVS. An HF band that covers frequencies between 0.5 and 30 Hz and the IP band that covers frequencies between 0.01 and 2.5 Hz. And to facilitate detection of events in a broad frequency band, a sophisticated detection and location package needs to be implemented at the analysis center. Automated processing techniques should be applied before human analysis.

## State of Health (SOH)

The state of health (SOH) information ensures the quality of the data before it is analyzed. It is divided into thirteen sections (Table 4). We looked at SOH to determine if all the information being collected is important and necessary and if any different information should be added.

SOH was evaluated in a number of ways. Daily checks of the SOH information were used to determine the status of the instrumentation. Currents and voltages were checked, along with temperatures of both equipment and vault areas. Calibrations of the seismometers were run approximately every 150 minutes. Data quality was checked by looking at the verification checksum. SOH information was also used for diagnostic purposes in the field. When the system would go down, things like the TEG voltages, battery

Table 4. State of Health Information

| frame | description |
|---|---|
| | **SITE MONITORS** |
| 00 | propane pressure |
| 01 | nitrogen pressure |
| 02 | propane level |
| 03 | TEG 1 voltage |
| 04 | TEG 2 voltage |
| 05 | TEG3 voltage |
| 06 | TEG bus current |
| 07 | module current |
| 08 | upper vault temperature |
| 09 | lower vault temperature |
| 10 | battery current |
| 11 | battery temperature |
| 12 | power dist. module temperature |
| 13 | 28 volt bus voltage |
| 14 | barometric pressure |
| 15 | wind speed |
| 16 | wind direction |
| 17 | relative humidity |
| 18 | outside temperature |
| 19 | building temperature |
| 20 | ice box door |
| 21 | shelter door |
| 22 | dome door |
| | **RECV/XMIT MONITORS** |
| 25 | HPA temperature |
| 26 | RT +12 |
| 27 | RT -15 |
| 28 | RT +5 |
| 29 | RT +15 |
| 30 | receiver signal level |
| 31 | HPA power |
| 32 | phase error |
| 33 | RT module current |
| 35 | antenna tilt |
| 36 | C-PLOLOCK |
| 37 | L-PLOLOCK |
| 38 | MODFAULT |
| 39 | DMODCARLOCK |
| 40 | BITSYNC |
| 41 | HPAPATH |
| 42 | DECODFAULT |
| 43 | DEMODFAULT |

| frame | description |
|---|---|
| | **TAPE MONITORS** |
| 50 | temperature |
| 51 | tape 1 +12 supply voltage |
| 52 | tape 2 +12 supply voltage |
| 54 | tape 1 +5 supply voltage |
| 55 | tape 2 +5 supply voltage |
| 57 | tape recorder current |
| 58 | RT HPA select |
| 59 | RT HPA on |
| 60 | recorder 1 power |
| 61 | recorder 2 power |
| 66 | recorder 1 full |
| 67 | recorder 2 full |
| 70 | recorder 1 error |
| 71 | recorder 2 error |
| 74 | % tape left in recorder |
| | **UPHOLE MONITORS** |
| 85 | +5 supply voltage |
| 86 | +5 return voltage |
| 87 | +12 supply voltage |
| 88 | +12 return voltage |
| 89 | -12 supply voltage |
| 90 | module current |
| 91 | temperature |
| 92 | delay board malfunction |
| 93 | delay board reset |
| 94 | delay memory error |
| 95 | SOH board malfunction |
| 96 | CPU reset |
| 97 | any comm. board reset |
| 98 | GPS satellite lock error |
| | **DHL MONITORS** |
| 115 | DHL chan. 1 malfunction |
| 116 | DHL chan. 1 comm. line error |
| 117 | DHL chan. 2 malfunction |
| 118 | DHL chan. 2 comm. line error |
| | **COMMAND MONITORS** |
| 140 | command echo byte 1 |
| 141 | command echo byte 2 |
| 142 | command echo byte 3 |
| 143 | command echo byte 4 |
| | **SEISMIC SOH** |
| 150 | Z mass position |

Table 4. State of Health Information (cont.)

| frame | description |
|---|---|
| 151 | N mass position |
| 152 | E mass position |
| 153 | calibration signal |
| 154 | pressure |
| 155 | temperature |
| 156 | carrier |
| 157 | carrier |
| 158 | G. clip |
| 159 | ZA voltage |
| 160 | NA voltage |
| 161 | EA voltage |
| 162 | ZC voltage |
| 163 | NC voltage |
| 164 | EC voltage |
| 165 | auxiliary voltage |
| | **DHL SOH** |
| 170 | -15 supply voltage |
| 171 | +15 supply voltage |
| 172 | +5 supply voltage |
| 173 | temperature |
| 174 | pressure |
| 175 | relative humidity |
| 176 | +5 return voltage |
| 177 | +15 return voltage |
| 178 | battery |
| 179 | osc. control voltage |
| 180 | tamper voltage |
| **TIMING STATUS REGISTER** | |
| 185 | slave / master mode |
| 186 | timing msg. transmit enable |
| 187 | update / routine msg. type |
| 188 | slave time error < 3 ms |
| 189 | update timing msg. ok |
| 190 | jamset this frame |
| 191 | master verify error |
| 192 | timing asynchronous |
| **OPERATING STATUS REG.** | |
| 195 | UHL/DHL comm. link ok |
| 196 | operate/install mode |
| 197 | system reset flag |
| 198 | system reset indicator |
| 199 | SDLC error flag |
| 200 | tamper detect |
| 201 | EEPROM & auth. keys erased |
| 202 | power failure recovery |
| | **CONTROL SOH** |
| 203 | verify byte ptr. VBALO |
| 204 | verify byte ptr. VBAHI |
| 205 | verify byte ptr. VBBANK |
| 206 | timing offset |
| 207 | timing DAC control |
| 208 | slave response byte SRB0 |
| 209 | slave response byte SRB1 |
| 210 | slave response byte SRB2 |
| 211 | slave response byte SRB3 |
| 212 | mode mod. counter |
| 213 | array element number |
| 214 | verify checksum |
| 215 | last msg. received MSBGT0 |
| 216 | last msg. received MSBGT1 |
| 217 | last msg. received MSBGT2 |
| 218 | last msg. received MSBGT3 |
| 219 | last msg. received MSBGT4 |
| 220 | last msg. received MSBGT5 |
| 221 | last updated SOH |
| | **HRD SOH** |
| 225 | HF Z sync |
| 226 | HF Z status |
| 227 | HF N sync |
| 228 | HF N status |
| 229 | HF E sync |
| 230 | HF E status |
| 231 | IP Z sync |
| 232 | IP Z status |
| 233 | IP N sync |
| 234 | IP N status |
| 235 | IP E sync |
| 236 | IP E status |
| **MISCELLANEOUS** | |
| 240 | spare |
| 241 | fixed data mode flag |
| 242 | AUTH test mode flag |
| 247 | HF HRD clip detect |
| 248 | IP HRD clip detect |
| 249 | data acquisition SOH |
| *repeat 150 through 249 for 2nd borehole* | |

voltages HPA power and receiver signal levels would be checked to determine where the problem occurred.

The time flag also part of the SOH information. The timing of DSVS at PSRF was good except for a period from September 10, 1991 through February 18, 1992 when the time was anywhere from ±30 seconds off. This was due to problems in the GPS satellite hardware and was corrected by implementing new software from Motorola. After February 1992 there were occasional problems with the time lock on the satellite, but they were fixed by the end of 1992.

The information collected in the SOH was valuable and useful in monitoring the system and keeping it running. The weather station and its SOH values was especially important in looking at the background noise. One area where there was not enough information was on the communications module. Sometimes there were difficulties in retrieving data from back-up tapes, and there was not enough information to determine why there was a problem. Two things would increase the usefulness of the SOH information; a real-time monitor and a paperless log of system problems. Both could be accomplished with a "semi" expert system that would monitor SOH in real time, warn the operator of problems and log the most probable reason for the problem (i.e. TEG voltage down, RT problem, etc.)

## Operational Characteristics

Since funds were not available to evaluate this system in an operational mode similar to the evaluation of the National Seismic Stations (NSS) in the Regional Seismic Test Network (RSTN), no real statistics were derived on operational performance. We would expect the performance to be similar to that of the NSS since the same design principles were followed. Statistics from the RSTN availability showed a data availability of 0.9992 and a mean time between failures (MTBF) of 2.08 years (Harrer, 1989). We do not imply that these statistics apply to the DSVS, only that the comparisons should be good.

## References


Bame, D., "Propagation of high frequencies in Scandinavia", SAND88-1047, 1989.

Bame, D.A., M. C. Walck and K. L. Hiebert-Dodd, "Azimuth estimation capabilities of the NORESS regional seismic array", Bull. Seism. Soc. Am., 80, 1999-2015, 1990.

Bame-Carr, D., "Discrimination using spectral slopes at frequencies up to 50 Hz", Bull. Seism. Soc. Am., 82, 337-351, 1992.

Basham, P. W. and K. Whitman, "Microseismic noise on Canadian seismograph records in 1962 and station capabilities", Pub. Dom. Obs. 32, 123-135, 1966.

Bungum, H., E. Rygg and L. Bruland, "Short period seismic noise structure at the Norwegian Seismic Array", Bull. Seism. Soc. Am., 61, 357-373, 1971.

Carr, D. B., "Azimuth estimation capabilities of the ARCESS regional seismic array", Bull. Seism. Soc. Am., (submitted for publication).

Chael, E. P., "Spectral discrimination of NTS explosions and earthquakes in the southwestern United States using high-frequency regional data", Geophys. Res. Lett., 15, 625-628, 1988.

"Deployable Seismic Verification Plan", DSVS Working Group, USDOE/NV, January 30, 1987.

Der, Z.A., A. O'Donnell, T. W. McElfresh, R. Jutila, J. A. Burnetti, M. Marshall, M. Silk and E. Gordon, "A study of seismic wave propagation at regional distances in five areas of the world", VSC-TR-82-14, 211pp, 1982.

Evernden, J. F., "Magnitude determination at regional and near regional distances in the United States", Bull. Seism. Soc. Am., 57, 591-693, 1967.

Fyen, J., "NORESS noise spectral studies and noise level characteristics" in NORSAR Semiannual Technical Summary 1 October 1986 - 31 March 1987, Scientific Report 2-86/87, 46-58, 1987.

Harrer, S. J., "Regional Seismic Test Network (RSTN) Operations Final Report", EGG-10617-6062, 92pp, 1989.

Magotra, N., N. Ahmed, and E. Chael, "Seismic event detection and source location using single station (three-component) data", Bull. Seism. Soc. Am., 77, 958-971, 1987.

Molnar, P. and J. Oliver, "Lateral variations of attenuation in the upper mantle and discontinuities in the lithosphere", J. Geophys. Res., 74, 2648-2682, 1969.

Ringdal, F. and H. Bungum, "Noise level variation at NORSAR and its effect on detectability", Bull. Seism. Soc. Am., 67, 479-492, 1977.

Roberts, R. G., A. Christoffersson and F. Cassidy, "Real-time event detection, phase identification and source location estimation using single-station three-component seismic data", Geophys. J., 97, 471-480, 1989.

Smart, E. and H. Sproules, "Detection of regional phases" in Preliminary Results of the VELA Seismological Center Research in FY80, AFTAC-TR-80-37, 85-91, 1980.

Taylor, S. R., 1981, "Properties of ambient seismic noise and summary of noise spectra in the vicinity of RSTN sites", UCID-18928.

Walck, M. C. and E. P. Chael, "Optimal backazimuth estimation for 3-component recordings of regional seismic events", Bull. Seism. Soc. Am., 81, 643-666, 1991.

Distribution:

US Department of Energy
Office of International Security Affairs
Attn: M. Koontz
L. Casey
D. Breding
Forrestal Bldg. IS-20
1000 Independence Ave. SW
Washington, DC 20585

Air Force Technical Applications Center
Attn: F. Pilotte (TT)
Lt. Col. M. Winchester (TTS)
Cpt. S. Doran (TTS)
Patrick AFB, FL 32925

Pinedale Seismic Research Facility
AFTAC Dept 489
Attn: D. Benedetti
Boulder, WY 82923

Advanced Research Projects Agency
Attn: R. Alewine
A. Ryall
Nuclear Monitoring Research Office
1400 Wilson Blvd.
Arlington, VA 22209

Lawrence Livermore National Laboratory
Attn: M. Denny
F. Followell
W. Hannon
P. Harben
K. Nakanishi
J. Zucca
P.O. Box 808
Livermore, CA 94550

Los Alamos National Laboratory
Attn: C. Newton MS335
S. Taylor MS335
T. Weaver
P.O. Box 1663
Los Alamos, NM 87545

US Dept. of Energy Nevada Field Office
Attn: J. O Donnell
P.O. Box 98578
Las Vegas, NV 89193-8518

USGS-Albuquerque Seismological Lab.
Attn: B. Hutt
J. Peterson
Bldg 10002
Kirtland ARB 87115

Center for Seismic Studies
Attn: G. Gustoffson
R. Blandford
Suite 1450
1300 North 17th Street
Arlington, VA 22209

Teledyne Geotech
Attn: O. D. Starkey
3401 Shiloh Rd.
Garland, TX 75040

EG&G Energy Measurements Inc.
Attn: J. Tsitouras MS570/D-12
P.O. Box 1912
Las Vegas, NV 89125

RSN
Attn: S. Thompson
P.O. Box Y5487
Las Vegas, NV 89193-5487

IRIS Headquarters
Attn: Rhett Butler
1616 North Fort Myer Dr. Suite 1440
Arlington, VA 22209

Dr. Roger Hansen
University of Colorado
Department of Physics
Joint Seismic Program Center
Campus Box 583
Boulder, CO 80309-0390

| | |
|---|---|
| 5004 | P. A. Stokes |
| 6114 | M. W. Scott |
| 6114 | E. F. Roseth |
| 6116 | M. C. Walck |
| 6116 | C. J. Young |
| 9200 | T. A. Sellers |
| 9201 | T. G. Taylor |
| 9204 | L. S. Walker |
| 9204 | D. B. Shuster |
| 9232 | B. N. Malm |
| 9236 | P. B. Herrington |
| 9236 | D. R. Breding |
| 9236 | D. B. Carr (5) |
| 9236 | E. P. Chael |
| 9236 | J. P. Claassen |
| 9236 | B. H. Corbell |
| 9236 | R. P. Fleming |
| 9236 | S. J. Harrer |
| 9236 | J. W. Walkup |
| 9311 | A. J. Chabai |
| 9311 | H. D. Garbin |
| 8523-2 | Central Technical Files |
| 7141 | Technical Library (5) |
| 7151 | Technical Publications |
| 7613-2 | Document Processing for DOE/OSTI (10) |

DATE
FILMED
10/27/93
END